ELSEVIER

Journal of Chromatography A 826 (1998) 1–13

JOURNAL OF CHROMATOGRAPHY A

Visualization of solute migration in liquid chromatography columns

R. Andrew Shalliker[a,b], B. Scott Broyles[a,b], Georges Guiochon[a,b,*]

[a]*Department of Chemistry, The University of Tennessee, Knoxville, TN 37996-1600, USA*
[b]*Chemical and Analytical Science Division, Oak Ridge National Laboratory, Oak Ridge, TN 37831-6120, USA*

Received 24 June 1998; received in revised form 7 September 1998; accepted 7 September 1998

Abstract

By matching the refractive indices of the mobile phase, the stationary phase and the material of the bed enclosure, one can render transparent to the eye the chromatographic column which is normally opaque in nature. As a result, band visualization is readily obtained. High-definition on-column detection becomes feasible by using a photographic detector instead of the conventional post-column, on-line (UV–Vis or similar) detector. Quantitative information regarding the concentration distribution in the band is obtained by utilizing optical scanners to obtain a digital image and computer imaging software. The processes of data collection and image analysis are discussed in detail and are illustrated by observing the concept of the infinite diameter column following a central point injection. The performance of the photographic detection method is compared to that of regular detection procedures. The efficiency of the column was determined with both on-column measurements and regular post-column measurements. A minimum reduced plate height (h) of 1.9 was recorded with post-column detection, in agreement with the average of the results given by on-column detection. On-column analysis allowed the determination of the local plate height which was found to vary across the central region of the column between 2.7 and 0.95.

Keywords: Detection, LC; Visualization of solute migration; Solute migration

1. Introduction

Three factors hinder the chromatographer from viewing in real time the profiles of the bands during their migration along the column. First, the material used to contain the stationary phase and channel the mobile phase through the bed is usually stainless steel, sometimes polyether ether ketone (PEEK), rarely a transparent substance. Second, if glass columns are employed, the opaque nature of a bed of silica particles prevents seeing what happens inside. Finally, if column tube and packing material were transparent, most analytes do not absorb visible light. As a result, studies centered around the determination of band profiles or the study of band dispersion have usually been carried out post-column. Little information can be gained on transverse dispersion or for that matter on the transverse heterogeneity of the packed bed. Furthermore, limited information may be obtained regarding the influence of sample introduction procedures and the effect that inlet and outlet frit geometries may have on the band shape. Even accurate information regarding the axial dispersion is limited because of extra-column effects.

*Corresponding author. Corresponding address: Department of Chemistry, The University of Tennessee, Knoxville, TN 37996-1600, USA.

0021-9673/98/$ – see front matter
PII: S0021-9673(98)00734-1

The possible regions of localized column heterogeneity cannot be determined. Any information we have regarding the actual behavior of a zone inside a column bed must be derived from inferences from the observation of the plates used in thin-layer chromatography (TLC) [1], an approach which is most insufficient.

It has been demonstrated that the transverse heterogeneity of packed beds is a significant source of band broadening [2–12]. The phenomenon, however, is difficult to observe and few studies have yet been undertaken in this field. Most evidences of this heterogeneity are circumstantial. Two types of studies have been conducted, the first using local detection at the column exit [2–9], the second using nuclear magnetic resonance (NMR) methods to measure the local properties of the bed (e.g., axial and transverse dispersion coefficient) [10–12] or to visualize the bands [13–15]. These studies have been reviewed recently [16] and need not be discussed in detail here again.

There is a general agreement that the radial flow profile experiences a range in local velocities across the column radius [2–9], that the ''wall effect'' plays an important role in band broadening, the local height equivalent to a theoretical plate (HETP) increasing several-fold from the core region to the wall region [2–9], and that the extent of the variation observed depends on the procedure used in the preparation of the column (columns prepared using a dry-packing method have a lower permeability in the core region [2,3], whereas the permeability of slurry-packed columns was lower at the wall [4–9]). Therefore, the rate at which a solute introduced into the center of the column migrates to the wall determines to a large extent the migration flow stream of a sample band. Hence, the dispersion of an elution band is also a function of the radial dispersion of the zone in the column bed and not simply a function of the axial dispersion. Knox and Parcher [17] and Knox et al. [2] were the first to evaluate transverse solute dispersion using end column polarographic detection. Their studies showed that point injection into the central region of the column allowed a solute to migrate along the column without reaching the wall if the following condition

$$\nu_{crit} = \frac{16B}{I - 16A_r} \tag{1}$$

is satisfied [2,3]. In Eq. (1), ν_{crit} is the critical reduced velocity (i.e., the reduced velocity below which a solute may disperse to the column wall before the elution of its band is complete), I is a dimensionless term defined by

$$I = \frac{d_c^2}{Ld_p} \tag{2}$$

where d_c and d_p are the column and average particle diameter, respectively, L is the column length, and B and A_r are the coefficients of the conventional HETP equation

$$h_r = \frac{B}{\nu} + A_r \tag{3}$$

where B/ν is the axial dispersion contribution to the reduced HETP and A_r is the contribution to radial dispersion originating from stream splitting [9,10,18]. For a given column diameter and particle diameter, the ability of a solute to migrate to the wall depends on the reduced velocity of the mobile phase and the length of the column. Ideally, for a point-like injection, the conditions may be varied such that a column behaves or not as an ''infinite diameter'' column [17], depending on the reduced velocity of the mobile phase. However, modern chromatographic columns have advanced in such a manner that their operation in the infinite diameter mode is all but impossible. Columns tend to be narrow and long, and valve injection disperses the sample across the column, to its wall almost immediately upon entry into the column. Central injection has been abandoned.

In this work, we discuss an alternative method for viewing the behavior of a solute band during its migration along the column. This method uses a glass column allowing the direct observation of the stationary phase. The refractive indices of the stationary and mobile phases are matched, so the opaque bed of adsorbent becomes transparent. Injection of a colored species or one with a different refractive index allows observation of the solute band. Kirkland [19] used this method to illustrate the ''infinite diameter'' column concept of Knox and Parcher [17] but did not collect information regarding chromatographic parameters, most likely because of the lack of the supporting technical imaging hardware and software that is available today. In a

previous report [20], we illustrated the usefulness of this technique for the visualization of viscous fingering. In this paper we illustrate how the use of proper hardware and software permits the transform of a simple photograph into a digital image of the zone from which a variety of important chromatographic parameters can be determined after scanning the image.

2. Experimental

2.1. Chemicals

All solvents were used as supplied by their manufacturers. Reagent grade carbon tetrachloride was purchased from Sigma (St. Louis, MO, USA). High-performance liquid chromatography (HPLC) grade dichloromethane and HPLC grade methanol were obtained from Fisher Scientific (Fairlawn, NJ, USA). Iodine (99.9%) was obtained from General Chemical Division (New York, NY, USA). The chromatographic stationary phase used was YMC 15–30 μm C_{18} chemically bonded silica (YMC, Wilmington, NC, USA).

2.2. Columns

All chromatographic experiments were performed on a 100 mm×17 mm borosilicate glass column supplied by Omnifit (Coldhams Lane, Cambridge, UK). The column end fittings were prepared by the workshop of the UT chemistry department. Columns were slurry-packed in a downward configuration, using dichloromethane as the displacement solvent, methanol as the slurry solvent, and methanol as the packing solvent, at pressures less than 400 p.s.i. (1 p.s.i.=6894.76 Pa) (so as not to shatter the glass or break the end fittings). An axial compression end fitting allowed some compression of the bed head and ensured that no voids were present at the column inlet nor formed during operation. The actual bed length of the column was 6.5 cm. Visualization was improved by submersion of the cylindrical glass column into a carbon tetrachloride reservoir in the form of a rectangular box with glass windows on each of its four lateral sides. This eliminated the effect of cylindrical lens during observation or photography of the column.

2.3. Sample injection

A saturated solution of iodine was used as the probe solute. In carbon tetrachloride this amounts to a concentration of approximately 26 g/l [21]. At this concentration, the solute band is highly colored and allows the observation of the small volumes injected, 20 μl in this work during their entire elution. Central point injections were made 0.5 cm below the bed head and were performed using a laboratory-made device and a Hamilton (Reno, NV, USA) syringe with the sharpened end filed flat.

2.4. Equipment

The chromatographic system consisted of two HPLC pumps (Model 510, Waters Associates, Milford, MA, USA) controlled by a Waters gradient profiler. A variable-wavelength UV detector (SpectroFlow 757) was set at 440 nm to record the chromatographic response. Data acquisition was obtained using a DOS based software (Peaksimple II version. 3.54, from SRI Instruments, Torrance, CA, USA) and an IBM 386 personal computer.

The photographic and imaging equipment consisted of two Pentax ZX-M SLR cameras fitted one with a Promaster 100-mm fixed focal length macro (f3.5), the other with a Makinon 80–200 mm macrozoom (f4.0) and a +4 adaptor. Hoya FL-W and Skylight (1A) filters were fitted to both lenses (THK Photo Products, Rancho Dominguez, CA, USA). The film used throughout this study was Kodak 200 ASA 35 mm slide film. A Nikon Coolscan II (Nikon, Melville, New York, NY, USA) was used to scan the color slides. SigmaScan Pro 4.01 (Jandel Scientific, San Rafael, CA, USA) and Adobe Photoshop 4.0.1 (Adobe Systems, San Jose, CA, USA) were used to view and analyze the digital images. A 200 MHZ Pentium MMX based personal computer with 128 MB of RAM was used for computing of the digital image and of the different scans needed.

2.5. Data analysis

The process of using the zone visible to the naked

eye in order to acquire meaningful, quantitative chromatographic data regarding the retention, the dispersion process of this zone, and the distribution of the local mobile phase velocity involves the following three basic steps: (1) photographing the zone with the two cameras located at right angles. (2) Converting the photographic band images into a digital images. (3) Analyzing the digital images with the appropriate imaging software.

It is critical that the integrity of the actual elution band is maintained throughout the process of data extraction. To that end, some important aspects of the analysis need to be adhered to. These are discussed in detail below for each of the three steps.

2.5.1. Photographic considerations

Due care must be taken during the photographing of the elution band. Optical distortion associated with the cylindrical lens effect from the chromatographic column itself would cause extreme image distortion. This effect was minimized by submersion of the column in a reservoir of carbon tetrachloride in the form of a rectangular box with four glass faces parallel to the column axis. The cylindrical lens effect is illustrated in the photograph shown in Fig. 1, where part of the column was submersed in carbon tetrachloride and part of the column was not. Without the submersion the stationary phase appears to extend nearly all the way or all the way to the outer wall, while with the submersion the inner wall can clearly be observed and its actual thickness measured. Note that, for the purpose of viewing the stationary phase in Fig. 1, the column was filled with methanol rather than carbon tetrachloride. When the column is flushed with carbon tetrachloride the stationary phase is no longer visible.

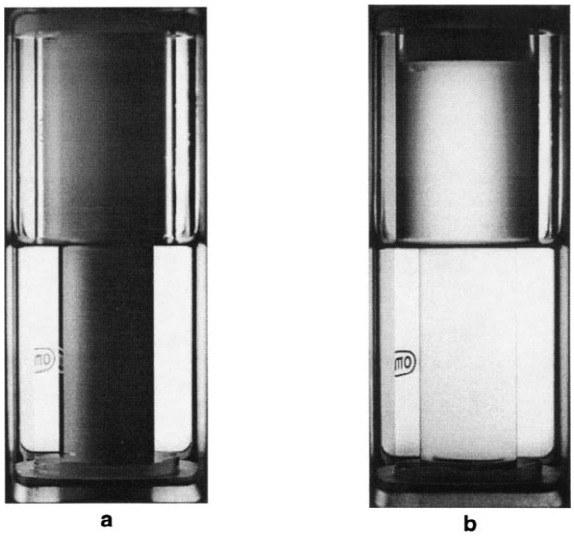

Fig. 1. Photograph illustrating the cylindrical lens effect using the reservoir half filled with carbon tetrachloride. (a) Column packed with C_{18} silica and filled with methanol. (b) Same column as in (a), but filled with carbon tetrachloride.

In these experiments, visualization of the band image is by transmission. That is, the light is absorbed during transmission through the column and the zone, if there is one. Photography fixes accurately the concentration distribution in the zone provided that the photographic process is carried out under linear conditions. It is therefore important that the lighting conditions be as uniform as possible. Soft, uniform lighting of the column was achieved by placing a frosted glass plate in two viewing ports of the column reservoir. Incandescent lighting behind these plates would have produced a non-uniform yellowish tinge to the photographic image, interfering unfavorably with the extraction of information. For that reason, fluorescent lighting was employed instead. This resulted in an unacceptable green discoloration of the image which was corrected by fitting a fluorescent filter FL-W to both camera lenses. A slightly pink image was obtained. This was acceptable because proper manipulation of the digital image allowed the subtraction of a background image, as discussed later.

Image asymmetry or distortion is likely when undertaking macro-photography. It must be carefully avoided. To this effect, high quality lens optics must be used and the apertures should be kept as small as possible. To further minimize image distortion, both lenses were used with apertures lower than f/16, which also helped to maintain a sufficient depth of field. Viewing of the photographic images confirmed the lack of either barrel or pincushion distortions in the photographs of the bands.

In order to obtain information regarding band uniformity and its three-dimensional profile, two cameras were employed in this study. They recorded images simultaneously, at right angles. Both cameras were synchronized to record the image at exactly the same time.

To limit the distortion of the image due to the movement of the band during exposure, these times were maintained below 1/125th of a second (0.008 s) at all times. The elution time of I_2 at 1.0 ml/min was 579 s, corresponding to a band velocity of $1.12 \cdot 10^{-4}$ m/s. Hence during an exposure lasting 0.008 s, the sample band moved 0.9 μm. This is well below the resolution of the digital conversion process, which is 20 μm (to be discussed later). As a result, the movement of the sample band during exposure was not a factor in the band shape. Fig. 2 illustrates the experimental set-up, showing the location of lighting and cameras in relation to the column.

Finally, there must be a linear relationship between the sample concentration, the intensity of the light beam hitting a point of the photographic film and the local density of the image. We assume the validity of Behr–Lambert law. The absorbance must be below 0.10 unit in order for the logarithmic dependence to be represented acceptably well by a linear one. The light intensity should not be excessive. These conditions were met in our experimental setting.

2.5.2. Digital transformation

Two methods may be employed to obtain a digital image. The first method is to use a digital camera to record directly a digital image, which can then be downloaded directly into the image analysis software. However, this procedure requires the services of a sophisticated digital camera. In order to photograph the image with the desired resolution, at an appropriate focal length, two SLR (single lens reflex) digital cameras would be required, at a cost which could not be afforded. As an alternative, we employed two standard, manual function and manual focus SLR optical cameras. A digital scanner was used to convert the photographic image to a digital form.

To achieve the highest possible cost effective resolution, the scanner employed was a slide/negative scanner manufactured by Nikon with a purchase price of approximately US$900. In all experiments slide film was used as we were advised this afforded better color reproduction and resolution during the scanning process than negatives. Using the Nikon scanner, the resolution achievable was on the order of 106.3 pixels/mm which equates to 9.4 μm/pixel. However, due to limitations imposed by the dimensions of the film and the magnification of the camera lenses, an effective resolution of 19 μm to 20 μm/pixel (effectively one particle diameter) was achieved. A better resolution was not desired since we were looking for parameters averaged over at least one particle volume.

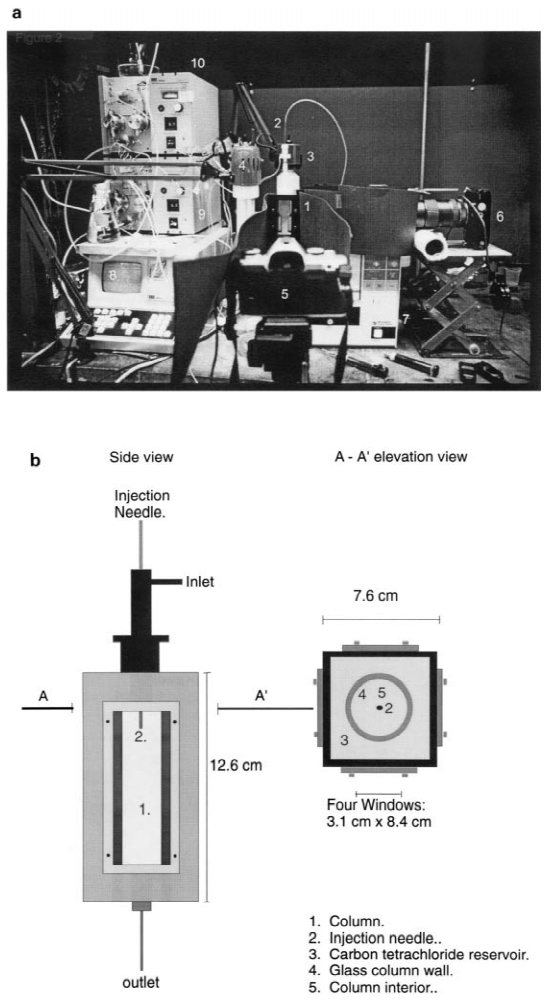

Fig. 2. (a) Photograph of the equipment illustrating the orientation of the cameras and lighting. 1 = Carbon tetrachloride reservoir and column, 2 = injection needle and tubing, 3 = light A, 4 = light B, 5 = camera A, 6 = camera B, 7 = UV–Vis detector, 8 = gradient controller, 9 = pump A, 10 = pump B. (b) Illustration of the column reservoir. The reservoir contains carbon tetrachloride. Viewing, lighting and photography of the column is possible through the glass windows cut into each side of the container.

The total image size after scanning was 2592×3888 pixels for maximum resolution. The dimensions of the scanned image containing the necessary information was approximately 920×3290 pixels. The reduction in useful image dimensions resulted from the need to include the entire column bed in the frame and the dimensions of 35 mm film. Switching to a larger film format to achieve better resolution was not a practical alternative for this work.

2.5.3. Profile imaging

Having obtained a digital image from the Nikon scanner, Adobe Photoshop and SigmaScan Pro were used to convert the band image into a set of numbers describing the concentration distribution in the zone. Considerable computing power was required for this purpose. Firstly, the uncompressed scanned image was imported into Adobe Photoshop to prepare the image for measurement. The true color image was converted to a 256 color grayscale image where a zero value represents total black and a value of 255 represents pure white. The values in between represent shades of gray. This conversion is necessary in order to perform the subtraction of the background image and for subsequent measurements in SigmaScan Pro. In order to reduce the contribution of the background to the overall grayscale histogram of the image, a grayscale converted color image of the column without an injected sample was subtracted from the grayscale image containing an injected sample band. This procedure produced an image with a relatively solid white background with a sharp contrasting dark toned sample band. A simple procedure can be employed to reverse the intensities of the background and the sample to light and dark respectively. Extreme care was used during the subtraction process to preserve the integrity of the sample band.

Once the subtraction was completed the image was cropped to remove excess portions of the image and to reduce the image file to a more manageable size (approximately five megabytes). In order to preserve image integrity, file compression was not used to reduce the file size. Finally, SigmaScan Pro software was used to measure the grayscale intensities along scan directions parallel to the axis of the column, from the needle tip down to the outlet frit.

3. Results and discussion

3.1. Band visualization

From a purely visual stand point, central point injection provided an ideal illustration of the process of band visualization by virtue of matched refractive indices and the subsequent extraction of chromatographic information. Fig. 3a and b illustrate the migration of an iodine band migrating with a stream of carbon tetrachloride, along the C_{18} silica column, after entering the column following a central point injection. These two photographs are shown without image manipulation. The injection volume was 20 μl and the photographs were recorded at 90° angles, immediately following injection and at the time of flow initiation. With the current injection design, the central point injection of the sample was performed in the absence of mobile phase flow. This was necessary because the needle, which did not have a frit was located 5 mm into the column packing. If the injection valve was opened in the presence of flow, column packing may flow into the needle and block the syringe thus destroying the bed. At all times during a central point injection, the flow was off when the outlet valve of the injection system was opened. With the injection valve closed, back pressure in the valve itself prevented particles from entering the needle and allowed the syringe to be permanently inserted into the column bed, thus increasing the life time of the column beyond the value that would have been expected otherwise if the syringe were to be removed for each injection. Maintaining the syringe within the bed also increased the reproducibility of an injection.

An interesting aspect of the band profile is the change in shape that occurred during band migration, an effect that is illustrated in Fig. 3a–f. Upon injection, the sample immediately was dispersed and diluted into a large, and almost perfect sphere (Fig. 3a and b). When flow was initiated, the trailing edge moved first and hence became flattened and the profile formed an inverted umbrella shape (Fig. 3c). After migration over approximately one third of the bed length, the band reformed to a nearly spherical shape (Fig. 3d). At the outlet of the column, dispersion of the band was obvious (Fig. 3e and f). Fig. 3e and f represent the same injection, but are collected

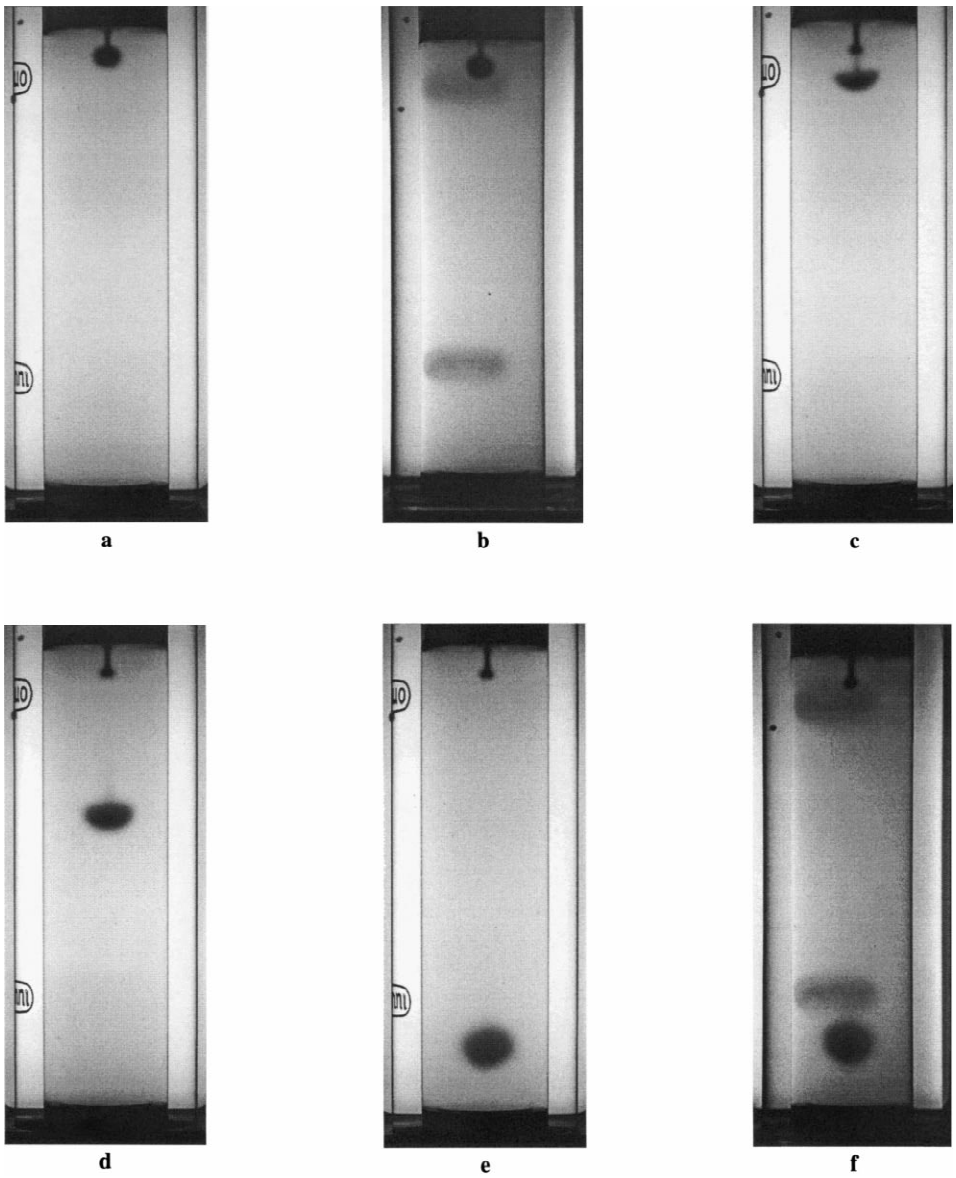

Fig. 3. Photograph of a central point injection (20 μl) of iodine in carbon tetrachloride. (a) and (b) Photographed from cameras mounted at right angles. (c) Photograph of the same injection showing the umbrella shaped band profile following flow initiation. (d) and (e) Photograph of the same band after migration along the bed at 2.1 cm and 5.2 cm, respectively and (f) is the right angle photograph of the band at the same location as (e). Flow-rate = 1.0 ml/min. Camera settings: aperture = f/16, shutter speed = 1/125. Film: Kodak 200 ASA slide film.

at 90° angles, showing that the band is highly symmetrical and nearly spherical. The transition in band shape from the inverted umbrella to a spherical form indicates that the axial dispersion of the band was most severe in the central axis of the column. However, this shape may also form if there was a flow region with a higher velocity between the central axis and the wall. Such a velocity distribution was observed by Farkas et al. [7–9] who reported the elution of crown shaped elution profiles following end column detection methods. However, as the length of our column was short, accurate measure-

ment of this phenomena was difficult to determine with certainty. Notice that as the sample band approached the outlet frit, flow variation in region of the frit caused the band to distort at the leading edge.

Importantly, the sample eluted from the column never having entered the wall region. In these experiments, the column behaved in the manner of an ''infinite diameter'' column. To the extent of our knowledge, only one other example of the infinite diameter column showing the sample band migration [19] has been reported.

3.2. Image manipulation

Quantitative information may be obtained following scanning of the image and subsequent background subtraction to produce a high quality digital image. For example, Fig. 4a–c illustrate this process for the sample band illustrated in Fig. 3e, which had traversed 5.2 cm of the bed. Notice in Fig. 4 that the OMNI logo is clearly visible in both Fig. 4a and b, but largely subtracted in Fig. 4c. Ideally, complete subtraction is sought as this verifies that the two images overlap identically. However, in reality, this is an extremely difficult task and some uncertainty in the result exists. The ramifications of this uncertainty are that firstly, the background coloring is not entirely removed, but, most importantly, limitations are placed on the accuracy to which measurements may be made in the close proximity of the wall region. With careful manipulation of the images we expect that this uncertainty is in the order of 5–10 particle diameters.

Another important aspect that should be noted at this time is that the image that we obtain is a two-dimensional photograph of a three-dimensional band. The image appears to be two-dimensional like a band on a TLC plate. However, the band profile is in fact a three-dimensional object, like a ball in a cylindrical column. Observation of the band profile from actual viewpoints located above and below it shows that the top and bottom sections of the band profile are hemispherical and that each side region is curved in the three-dimensional space. These views are difficult to photograph, but the shape is obvious to the eye. By comparing photographs in two orthogonal planes, the three-dimensionality is confirmed. In the following discussions we refer to the column

Fig. 4. (a) Digitized image of the photograph recorded in Fig. 3e. (b) Digitized image of a photograph of the column with only carbon tetrachloride and no sample present. (c) Digitized image of the photograph in Fig. 3e following the background subtraction of Fig. 4b from Fig. 4a. The resulting Fig. 4c is a digitized image corrected for the background color.

as having a right hand side (+ve) and a left hand side (−ve). This notation refers to the image as viewed from the camera from which that particular information is derived.

Finally, we should note that the apparent path length is slightly disturbed because the refractive index of the borosilicate glass is not exactly the same as that of the stationary phase and the carbon tetrachloride, hence some band distortion may occur. We believe that this distortion is minor because the refractive index of the glass is 1.473 compared to 1.466 for carbon tetrachloride. However, the extent of this distortion is at present unknown. We are currently investigating methods to determine this effect, but the problem is complicated because the injection plug is not a uniform solid cylindrical plug. Future communications will evaluate this problem.

3.3. Image scanning and determination of absorbance profiles

Once a digital image has been obtained, the image file can be analyzed using a software imaging program. We used Sigma ScanPro in conjunction with Adobe Photoshop. An enormous number of possibilities arise for the analysis of such a profile using these software packages. However, we are primarily concerned with transforming this image into a series of chromatographic profiles. The intensity of the black and white color scale was evaluated along the entire length of the column from the injection needle to the outlet frit. This resulted in the histogram shown in Fig. 5a. This chromatogram shows the concentration distribution along a narrow band, parallel to the column axis, along the central region of the column. This band was 15 pixels wide (corresponding to approximately 15 particle diameters). The noise level is rather high, with a signal-to-noise ratio in the order of $S/N=40$. It results in part from the high density of the data points acquired: there are 3174 data points in this chromatogram, approximately 600 data the 1.1 cm band width at baseline. With such a high sampling rate, a high noise level should be expected. In order to decrease the noise two solutions are possible. Firstly, the width of the sampling band could be increased. Increasing it from 15 pixels to 101 pixels decreased the noise significantly (Fig. 5b). However, with this method of noise reduction, the width of an individual analysis region increased and fewer sections of the column could be analyzed without sample line overlap. A second method of noise reduction was by smoothing the band. In Fig. 5c, the moving average of 25 successive data points was plotted versus the distance. The result was a much improved S/N ratio for a sampling band of 15 pixels.

Profiles similar to those in Fig. 5c can now be acquired by scanning the image systematically along bands parallel to the column axis. Fig. 6a and b illustrate the profile of the sample band already shown in Fig. 4. Fig. 6a represents the region of the left hand side of the column while Fig. 6b represents the right hand side. These plots show that following a central point injection, under such conditions that migration follows the infinite-diameter column model, the retention time remains nearly constant, practically independent of the radial location and, most importantly, that band broadening did not increase at the extremities of the plug. One of the niceties associated with on-column analysis of the migrating band profile is that the band can be visualized and represented in a three-dimensional contour plot. Fig. 7 illustrates a three-dimensional view of the sample band following central point injection after it has migrated 52 mm along the bed. This profile appears somewhat similar to those previously reported by Yun et al. [22] where the theoretical band shape was modeled for various centrally injected profiles.

Because the sample injection band was immediately dispersed and diluted during the process of injection, the total dispersion (σ_T^2) is the sum of the dispersion contributions originating from the injection process (σ_i^2) and from the dispersion in the packed bed (σ_c^2). However, because the band underwent a drastic change in shape as the flow was initiated, we can not simply measure the dispersion at the injection needle. Instead, once the profile has achieved a steady state in relation to the flow stream, the variance of the band at that location may be subtracted from the variance of the band at a location near the column exit to determine the contribution of the dispersion along the column. This yields the dispersion caused by the band migration along that region of the packed bed, without any contributions

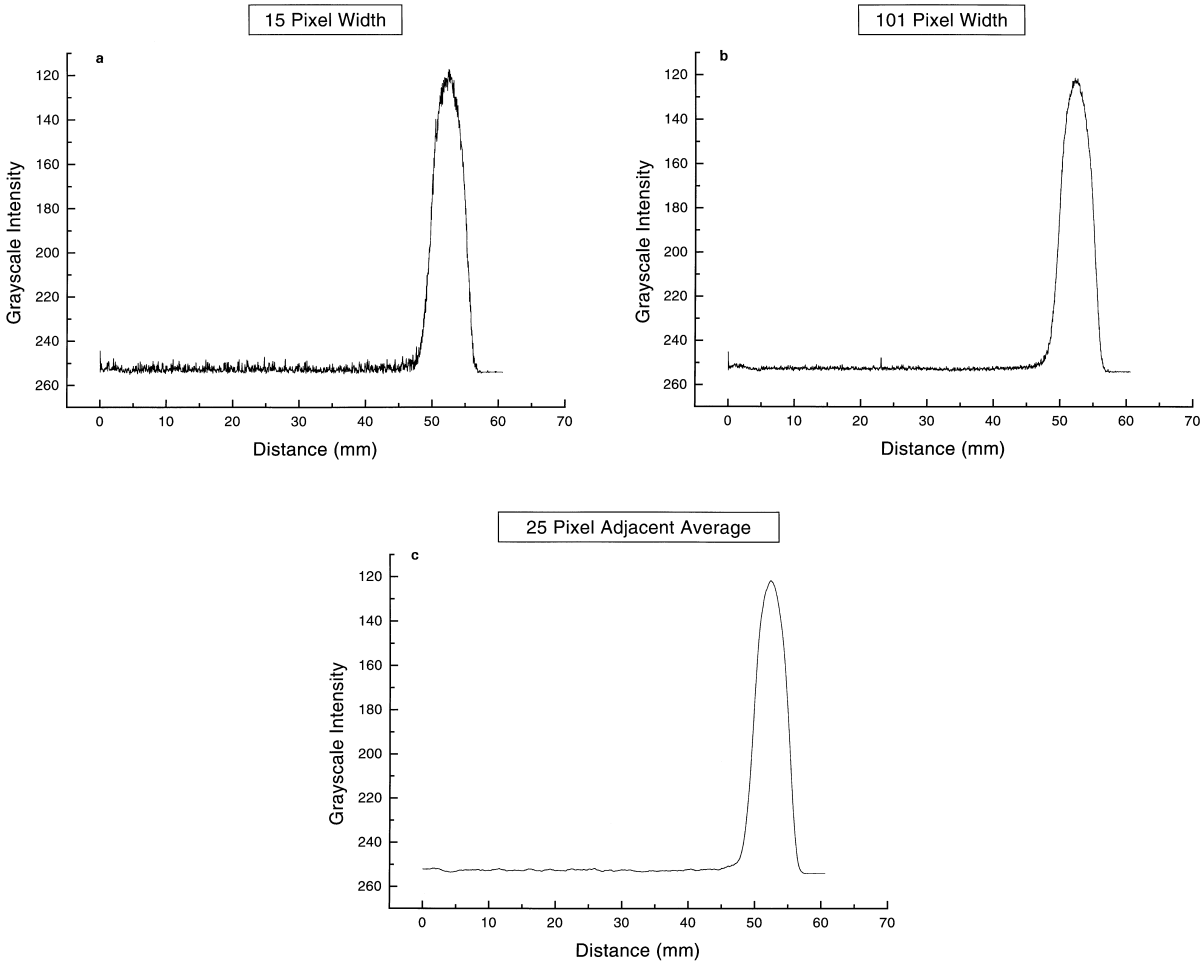

Fig. 5. Illustration of the band profile obtained from the histogram of light intensity across the digitized image produced in Fig. 4c. (a) Histogram obtained by measuring a band width of 15 pixels, (b) histogram obtained by measuring a band width of 101 pixels, and (c) histogram following adjacent averaging (25 points) of the histogram obtained in Fig. 4a.

from extra column effects. From that, the efficiency of the column is derived

$$N = \frac{L^2}{\sigma_c^2} \tag{4}$$

where L is the length of the bed between the position of the two images from which the variances have been measured.

Table 1 contains information relating the axial reduced plate height (h_a) at various radial locations across the column. The data was collected from both cameras, noted as camera (a) and camera (b). [The migration profiles shown in Figs. 6 and 7, for example, were collected by camera (a)]. In the center region of the column, a reduced plate height as low as 0.95 was determined from the information photographed by camera (a). Nowhere over the analysis region did the reduced plate height exceed 2.7. The average value measured from camera (a), over 21 tracks parallel to the column axis and located one along this axis, and 10 on each side of the axis, tiling approximately 6.0 mm of the band, was 1.71. Similarly, for camera (b), except that 17 tracks were measured and not 21, tiling approximately 4.7 mm of the band, the average was 2.24. The total averaged

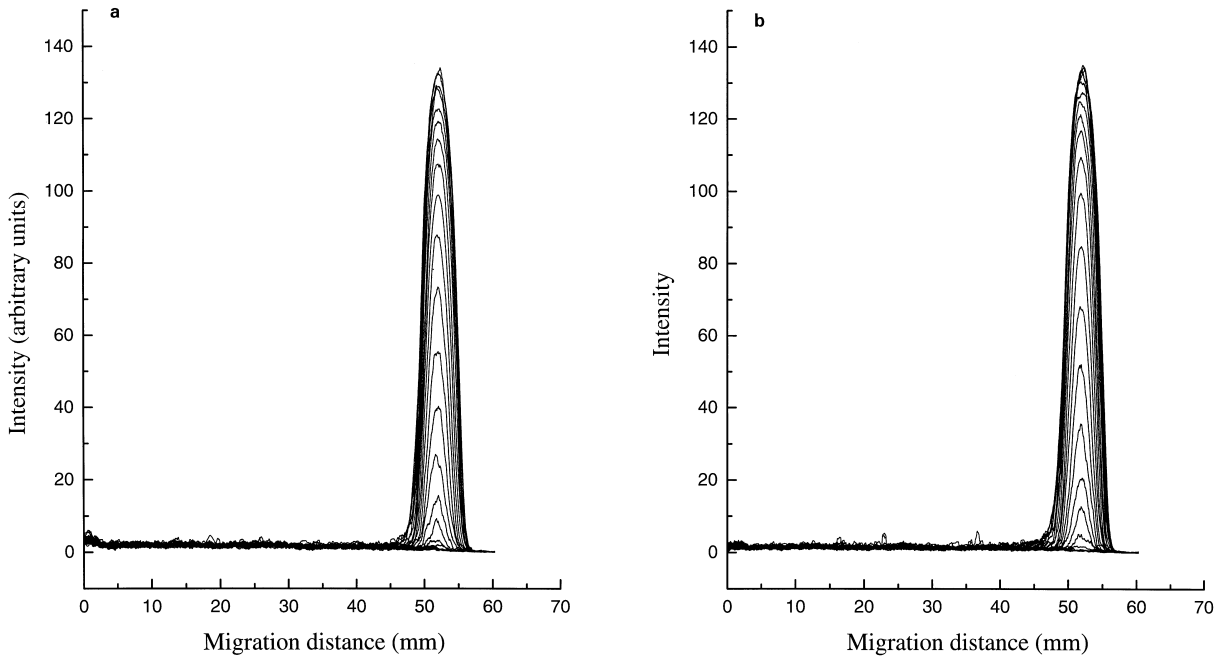

Fig. 6. Band profiles obtained from the histograms measured over the sample band illustrated in Fig. 3e. (a) Represents the left hand side and (b) represents the right hand side. Each profile was measured at radial locations every 16 pixels. Each band represents a surface of 15 pixels wide or 285 μm (approximately 15 particle diameters The image was divided into 31 sections radially across the column.

reduced plate height for 38 samples was 1.94. The very low reduced plate height just reported for the central region of the band from camera (a) may be an artifact and was not supported by the results from camera (b).

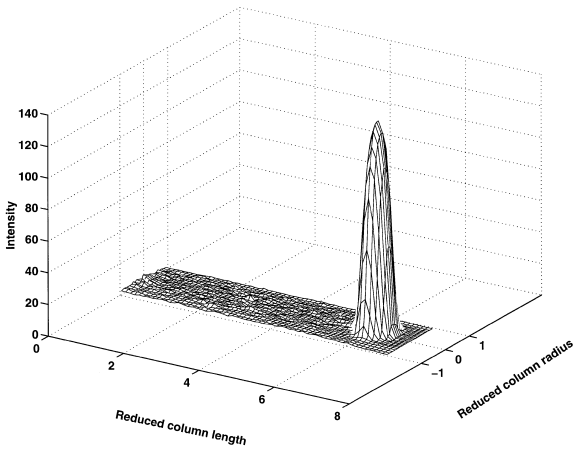

Fig. 7. Three-dimensional image of the sample band photographed after migrating 5.2 cm along the column.

One problem associated with our device for central point injection was that a very small quantity of sample leaked slowly from the needle after the injection was completed. This resulted in a tail forming at the rear of the band in the central region. When calculating the variance of the band, this tail skewed the histogram extracted from the intensity of the image. The result is an increase of the variance of the band closest to the injector because the tail had dispersed less and the color intensity was higher. As a consequence, the apparent number of theoretical plates for the region of the column downstream was too high. The leakage affects the data obtained from camera (b) less because the light exposure of this camera was set one half stop lower than camera (a). As a result the tail was barely visible, hence the skewness of the band was not as significant. Fig. 8 illustrates the radial variation of the local column efficiency in central point injection. The scatter of the results recorded from camera (a) is greater on the right hand side of the column, but most of the values are below 2. Overall, the plots of reduced plate height versus radial location follow the same trends

Table 1
Column efficiency following a central point injection

Radial position from center (mm)	Camera (a)		Camera (b)	
	Migration distance (mm)	*h*	Migration distance (mm)	*h*
2.921	51.85	1.22		
2.629	51.95	1.52		
2.337	51.79	1.56	50.50	1.87
2.045	51.59	2.03	50.12	2.16
1.753	52.06	1.76	50.64	2.28
1.461	51.81	2.00	50.48	2.46
1.170	51.89	1.27	50.38	2.42
0.888	51.98	1.94	50.46	2.40
0.585	52.10	1.56	50.52	2.35
0.292	52.33	0.95	50.58	2.47
0	52.38	1.78	50.56	2.62
−0.292	52.10	2.04	50.94	2.73
−0.585	51.78	2.38	50.72	2.66
−0.888	51.83	2.16	50.8	2.54
−1.170	52.23	2.18	50.82	2.31
−1.461	52.04	2.04	50.82	2.04
−1.753	52.04	1.70	50.7	1.88
−2.045	51.97	1.84	50.54	1.58
−2.337	52.06	1.56	50.48	1.37
−2.629	51.89	1.32		
−2.921	52	1.06		

and the two planes offer very similar results. For both planes, on the left hand side of the column, a distinctive trend exists where the efficiency decreased as the radial distance from the column center increased. The same trend was observed on the right hand side of the column, but the scatter of data from camera (a) makes this trend less significant. This result could seem to be in contradiction with those reported in all previous studies of the radial distribution of the column efficiency [2–9]. However, it should be emphasized that the data in Table 1 Fig. 8 were measured only in the central core region of the column (approximately between $r=0$ and $r=R/3$), far away from its wall. The phenomenon observed is new and interesting but not at significant variance from previous observations.

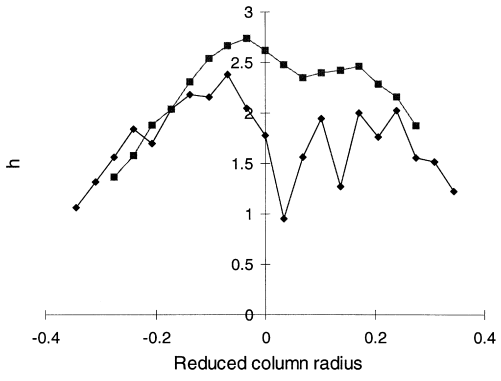

Camera (a) = diamonds.
Camera (b) = squares.

Fig. 8. Plot of reduced plate height versus radial location following a central point injection.

The elution profile of the centrally injected sample, recorded with a conventional bulk detector is shown in Fig. 9. The asymmetry factor for the profile shown is equal to 1.00. When the efficiency was measured from the variance or second moment of the chromatogram, the reduced plate height was determined to be 1.94. This is in exact agreement with the reduced plate height measured from the photographic image (averaged over 38 samples), indicating that useful chromatographic data may be obtained from this method of analysis.

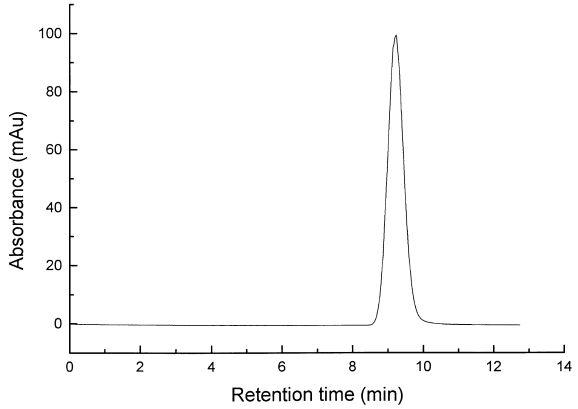

Fig. 9. Chromatogram of the same iodine sample as for the central point injection shown in Fig. 3. The chromatogram was measured with a standard UV–Vis bulk detector set at 440 nm with a 0.5 s rise time. Data acquisition was at 2 Hz. Chromatographic conditions as in Fig. 3.

4. Conclusions

Visualization of a sample band in real time is possible using the technique described. Most importantly, however, by careful manipulation of the photographic image and subsequent conversion to digital data, chromatographic data can be obtained with precision and accuracy. Dispersion was one particularly important parameter that was extracted from the photographic image. Consequently, the contribution of the column bed to its efficiency could be determined directly and detailed studies regarding localized column performance can be made. Detailed studies on the axial and radial dispersion for a variety of columns packed using different methods and with different packing materials are in progress.

As an example of the usefulness of this technique, the current work highlights the most impressive column performance associated with a central point injection. Even though conventional detection allowed this performance to be evaluated, visualization of the band allowed direct inspection and permitted the measurement of the local efficiency.

Acknowledgements

This work was supported in part by Grant DE-FG05-88ER13859 of the US Department of Energy and by the cooperative agreement between the University of Tennessee and the Oak Ridge National Laboratory.

References

[1] F. Geiss, Dünnschichtchromatographie, Hüthig, Heidelberg, 1989.
[2] J.H. Knox, G.R. Laird, P.A. Raven, J. Chromatogr. 122 (1976) 129.
[3] C.H. Eon, J. Chromatogr. 149 (1978) 29.
[4] J.E. Baur, E.W. Kristensen, R.M. Wightman, Anal. Chem. 60 (1988) 2334.
[5] J.E. Baur, R.M. Wightman, J. Chromatogr. 482 (1989) 65.
[6] T. Farkas, J.Q. Chambers, G. Guiochon, J. Chromatogr. A 679 (1994) 231.
[7] T. Farkas, M.J. Sepaniak, G. Guiochon, J. Chromatogr. A 740 (1996) 169.
[8] T. Farkas, M.J. Sepaniak, G. Guiochon, AIChE J. 43 (1997) 1964.
[9] T. Farkas, M.J. Sepaniak, G. Guiochon, Anal. Chem. 69 (1997) 4592.
[10] U. Tallarek, E. Baumeister, K. Albert, E. Bayer, G. Guiochon, J. Chromatogr. A 696 (1995) 1.
[11] U. Tallarek, K. Albert, E. Bayer, G. Guiochon, AIChE J. 42 (1996) 3041.
[12] U. Tallarek, E. Bayer, G. Guiochon, J. Am. Chem. Soc. 120 (1998) 1494.
[13] L. Plante, P. Romano, E. Fernandez, Chem. Eng. Sci. 49 (1994) 2229.
[14] M. Dickson, T. Norton, E. Fernandez, AIChE J. 43 (1997) 409.
[15] E. Fernandez, T. Norton, W. Jung, J. Tsavalas, Biotechnol. Prog. 12 (1996) 480.
[16] G. Guiochon, T. Farkas, H. Guan-Sajonz, J.-H. Koh, M. Sarker, B.J. Stanley, T. Yun, J. Chromatogr. A 762 (1997) 83.
[17] J.H. Knox, J. Parcher, Anal. Chem. 41 (1969) 1599.
[18] J.C. Giddings, Dynamics of Chromatography, Marcel Dekker, New York, 1964.
[19] J.J. Kirkland, in: N.J. Fina (Ed.), Proceedings of the First Philip Morris Scientific Symposium, Philip Morris, New York, 1973.
[20] B.S. Broyles, R.A. Shalliker, D.E. Cherrak, G. Guiochon, J. Chromatogr. A, in press.
[21] The Merck Index, Merck, Rahway, NJ, 10th ed., 1983, p. 4977.
[22] T. Yun, M.S. Smith, G. Guiochon, J. Chromatogr. A 828 (1998) in press.